Designing multifunctional CoO_x layers for efficient and stable electrochemical energy conversion

Matthias Kuhl,[a] Alex Henning,[a] Lukas Haller,[a] Laura I. Wagner,[a] Chang-Ming Jiang,[a,b] Verena Streibel,[a] Ian D. Sharp,[a,*] and Johanna Eichhorn[a,*]

[a] Walter Schottky Institute and Physics Department, Technical University of Munich, Am Coulombwall 4, 85748 Garching, Germany

[b] Department of Chemistry, National Taiwan University, 106 Taipei, Taiwan, R.O.C.

*Corresponding Authors: sharp@wsi.tum.de, johanna.eichhorn@wsi.tum.de

Abstract

Disordered and porous metal oxides are promising as earth-abundant and cost-effective alternatives to noble-metal electrocatalysts. Herein, we leverage non-saturated oxidation in plasma-enhanced atomic layer deposition to tune structural, mechanical, and optical properties of biphasic CoO_x thin films, thereby tailoring their catalytic activities and chemical stabilities. To optimize the resulting film properties, we systematically vary the oxygen plasma power and exposure time in the deposition process. We find that short exposure times and low plasma powers incompletely oxidize the cobaltocene precursor to $Co(OH)_2$ and result in the incorporation of carbon impurities. These $Co(OH)_2$ films are highly porous and catalytically active, but their electrochemical stability is impacted by poor adhesion to the substrate. In contrast, long exposure times and high plasma powers completely oxidize the precursor to form Co_3O_4, reduce the carbon impurity incorporation, and improve the film crystallinity. While the resulting Co_3O_4 films are highly stable under electrochemical conditions, they are characterized by low oxygen evolution reaction activities. To overcome these competing properties, we applied the established relation between deposition parameters and functional film properties to design bilayer films exhibiting simultaneously improved electrochemical performance and chemical stability. The resulting biphasic films combine a highly active $Co(OH)_2$ surface with a stable Co_3O_4 interface layer. In addition, these coatings exhibit minimal light absorption, thus rendering them well suited as protective catalytic layers on semiconductor light absorbers for application in photoelectrochemical devices.

Introduction

Electrochemical water splitting is a promising method to transform renewable energy into storable chemical fuels.[1–3] Earth-abundant electrocatalysts, such as transition metal oxyhydroxides and oxides, have attracted significant interest as efficient and cost-effective alternatives to noble-metal water splitting electrocatalysts, with importance for commercialization of large-scale energy storage devices.[4–6] Generally, optimal electrocatalysts need to fulfil several requirements, including chemical stability for long-term operation, sufficient conductivity to enable charge transfer, and intrinsic activity of catalytic sites for efficient energy conversion. In the past decade, efforts have been devoted to material development and structural design of non-noble metal catalysts to enhance their electrocatalytic activities. In this context, highly disordered and porous materials provide higher electrocatalytic activity given their increased concentrations of active sites and larger effective surface areas.[7,8] However, these materials often suffer from poor stability under operating conditions due to a variety of factors, including (electro)chemical susceptibilities and poor adhesion to the support structure. Therefore, catalyst-support integration and interface engineering play important roles for the realization of highly active and stable catalytic layers.

Interface engineering is especially important for the integration of such electrocatalysts with semiconductor light absorbers for solar-to-chemical energy conversion. In this regard, interfacing semiconductor light absorbers with conformal and ultra-thin catalytic layers is a promising strategy to overcome the poor efficiency and material stability of the semiconductor photoelectrodes under harsh photoelectrochemical operating conditions.[9–16] These multifunctional layers provide protection against corrosion in chemical environments and at the same time activate the desired catalytic reaction, while still permitting efficient interfacial charge transport and minimizing losses due to parasitic light absorption. However, simultaneously fulfilling each of these criteria requires precise control over film properties, often down to the sub-nm length scale. In this context, plasma-enhanced atomic layer deposition (PE-ALD) has emerged as a powerful method for designing surface and interface layers with tailored functionality and

accurate thickness control.[13–17] In PE-ALD, the deposited precursor is exposed to highly reactive plasma radicals and thus less thermal energy is required to drive the surface chemistry compared to conventional ALD. Consequently, PE-ALD has the advantage of partially decoupling metalorganic precursor oxidation kinetics from the substrate temperature, thereby providing access to a broader range of stable and metastable film phases, compositions, and properties.

To tune the material properties of PE-ALD thin films, the substrate temperature is still the most comprehensively investigated process parameter.[15,16,18] For the growth of multifunctional CoO_x films, it has been shown that low temperatures are not sufficient to completely decompose the precursor and lead to the formation of $Co(OH)_2$. In contrast, high substrate temperatures lead to complete oxidation of the precursor and yield structurally robust Co_3O_4 films.[15] The formation of simultaneously active and stable biphasic $Co(OH)_2/Co_3O_4$ films was only observed for intermediate substrate temperatures. In this case, the Co_3O_4 interface layer improves the durability of the substrate/catalyst interface due to its phase stability, while the $Co(OH)_2$ surface layer significantly enhances the rate of the electrocatalytic oxygen evolution reaction (OER) due to its facile *in situ* transformation to CoOOH.[19] For this case, empirical optimization of deposition temperature allowed the resulting biphasic films to reach a reasonable balance between catalytic efficiency and chemical stability. While this example highlights how incomplete oxidation can be leveraged to engineer functional metal oxide films via PE-ALD, precise control over the phase content of films, as well as their electrochemical characteristics, remains lacking. In addition, since plasma parameters are usually developed with the aim of ensuring saturated surface oxidation reactions, new opportunities lie in exploring how less aggressive plasma exposures can be used to precisely tailor the functional properties of metal oxide coatings. Here, we use oxygen plasma exposure time (t_{plasma}) and plasma power (P_{plasma}) to tune the phase and composition, as well as physical, mechanical, optical, and electrochemical properties of PE-ALD grown bifunctional CoO_x thin films at low substrate temperatures. Shorter t_{plasma} and lower P_{plasma} result in partial precursor oxidation, resulting in the incorporation of carbon impurities and the formation of highly porous films with weak substrate adhesion. In contrast, long t_{plasma} and high P_{plasma} completely oxidize the cobaltocene ($CoCp_2$) precursor, yielding CoO_x films with improved crystallinity and increased surface roughness, but also oxidize the underlying silicon support material. Both plasma parameters have a similar impact on the electrochemical performance and stability. Short pulses and low plasma powers lead to the formation of unstable, catalytically active $Co(OH)_2$ layers, while long pulses and high powers facilitate the formation of stable, inactive Co_3O_4 films. Catalytically active and highly stable biphasic layers consisting of a $Co(OH)_2$ surface layer and a Co_3O_4 interface layer are only formed for intermediate deposition parameters. The changes in chemical composition are also reflected in the optical properties of the CoO_x films, whereby parasitic light absorption in multilayer photoelectrodes is reduced for PE-ALD layers deposited with shorter plasma exposure times. The established relation between deposition parameters and functional properties of CoO_x films was successfully applied to control the surface/interface layer ratio and to design bilayer films with improved electrochemical performance without sacrificing chemical stability at a moderate current densities. Overall, this work highlights that an unsaturated oxidation of metalorganic complexes allows access to different material phases with tailored properties for engineering active catalysts and their interfaces.

Results and Discussion

Growth, Morphology and Electrochemical Properties

CoO_x thin films were deposited by PE-ALD on p^+-Si substrates using cobaltocene as Co precursor and oxygen plasma as oxidant. In the first half-cycle, $CoCp_2$ adsorbs on the substrate surface and, in the second half-cycle, reacts with oxygen radicals generated by the remote plasma. When the surface reaction is driven to completion, spinel Co_3O_4 is formed and CO_2, CO, and H_2O are released as gas-phase products.[16,20] For all PE-ALD growth processes investigated here, both the substrate temperature (100 °C) and the deposition parameters for the first half cycle were kept constant. To investigate how non-saturated oxidation reactions can be used to tune catalytic activity, chemical stability, and physical properties, the oxygen plasma exposure time was varied during the second half cycle from 5 s to 90 s at a constant plasma power of 10 W and, in a separate series, the plasma power was varied from 10 W to 300 W at a constant t_{plasma} of 5 s.

In-situ ellipsometry measurements were performed to understand the effect of t_{plasma} and P_{plasma} on the growth process (Fig. 1). For short t_{plasma} up to 10 s, a steady-state growth is observed starting from the first cycle (Fig. 1a). For

$t_{plasma} \geq 15$ s, the apparent thickness increase is faster in the beginning and settles to a constant linear increase for prolonged deposition times. The initial super-linear growth can be assigned to interfacial SiO_x formation.[21] In this initial period, the SiO_x formation increases with increasing t_{plasma} from ~5 cycles for t_{plasma} = 15 s to ~25 cycles for t_{plasma} = 90 s. In the steady state linear growth regime, the thickness increase upon $CoCp_2$ exposure is lower for shorter plasma exposure times (Fig. 1b), which indicates a reduced number of available binding sites for the precursor adsorption on the surface. During the subsequent purge step, the film thickness remains constant and decreases when the surface is exposed to oxygen plasma in the following step. During plasma exposure, the ligands are removed and the reaction of Co with oxygen occurs to form CoO_x. For short t_{plasma}, the small change in film thickness during plasma exposure indicates incomplete gas-solid oxidative interactions, which is also consistent with the observed decrease of available $CoCp_2$ adsorption sites in the subsequent cycle.

The different growth behaviors are also reflected in the growth per cycle (GPC) (Fig. 1c), which is defined as the thickness change per ALD cycle in the linear growth regime. Short exposure times of 5 s exhibit a low GPC, while the GPC is significantly higher for t_{plasma} = 10 s, but decreases for longer plasma exposure times. A higher GPC for short pulse times has been previously attributed to a redeposition of incompletely oxidized reaction products on the surface[22], which is reduced for increasing plasma exposure times. The change in GPC is consistent with the variation in film thickness as determined by X-ray reflectivity (XRR) and *ex-situ* variable angle spectroscopic ellipsometry (VASE, Fig. S1). Accordingly, we observe that at a plasma power of 10 W and substrate temperatures of 100 °C, a plasma exposure time of ≥ 15 s is required to achieve sufficient ligand oxidation and suppress redeposition of reaction products during CoO_x films formation.

In-situ ellipsometry was also conducted as a function of oxygen plasma power using a constant plasma exposure time of 5 s (Fig. 1d). Interestingly, the increasing plasma powers and plasma exposure times have a similar impact on the PE-ALD growth process. At low plasma powers ≤ 20 W, the thickness increases linearly for all deposition cycles, while for $P_{plasma} \geq 50$ W two different growth regimes are observed, consistent with interfacial SiO_x formation (Fig. 1d). The slow thickness increase for low plasma powers indicates limited availability of binding sites (Fig. 1e) and the faster growth rates for intermediate plasma powers are consistent with reaction product redeposition (Fig. 1f). While plasma powers of ≥ 50 W are necessary to reach saturated oxidation reaction conditions at 100 °C substrate temperature (Fig. 1e), lower plasma powers have the advantage of reducing interfacial oxide formation.

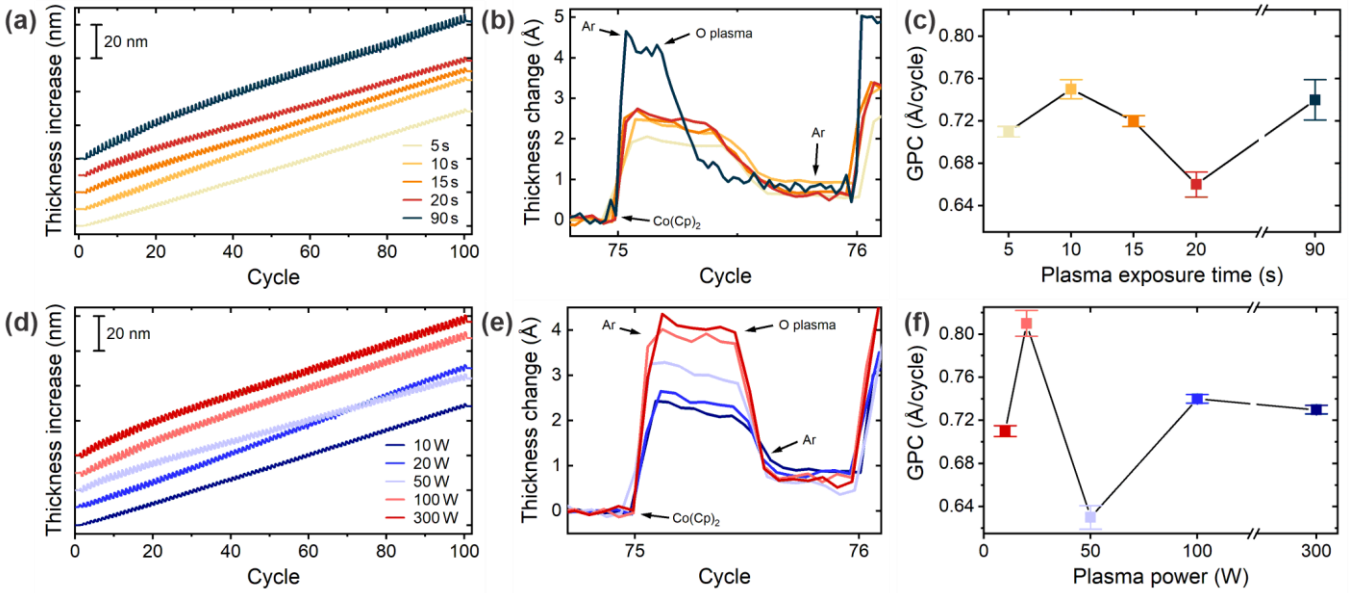

Figure 1. Growth characteristics of CoO_x thin films for increasing plasma exposure times and increasing plasma power. (a) Thickness increase as a function of deposition cycles measured by *in-situ* ellipsometry for increasing t_{plasma}. Curves have been vertically offset for clarity. (b) Corresponding, thickness changes over a single deposition cycle in the linear growth regime. Arrows indicate the start of different PE-ALD steps within a single cycle for t_{plasma} = 90 s. The injection points change for shorter plasma exposure times. (c) The growth per cycle extracted from the *in-situ* ellipsometry data in (a). (d) Thickness increase as a function of deposition cycles for increasing P_{plasma}. Curves have been vertically offset for clarity. (e) Corresponding, thickness changes over a single deposition cycle in the linear growth regime. Arrows indicate the start of different PE-ALD step. (f) The growth per cycle extracted from the *in-situ* ellipsometry data in (d).

For all plasma exposure times at a constant power of 10 W, atomic force microscopy (AFM) confirms the formation of planar and conformal layers (Fig. 2a). Increasing oxygen pulse times from 5 s to 90 s slightly increases the surface roughness from 0.24 nm to 0.35 nm, which is similar to or lower than previous reports on PE-ALD grown Co_3O_4.[15,16,23] For longer plasma exposure times, the grain-like structure is more pronounced. Consistent with this observation, complementary grazing incidence X-ray diffraction (GIXRD) measurements show the appearance of weak diffraction peaks for plasma exposure times of 15 s and longer, corresponding to the formation of Co_3O_4 (Fig. S2). From these observations, it can be concluded that the crystallinity of the PE-ALD films is increased for prolonged plasma exposure, which leads to increased surface roughness and more pronounced grain structure observed by AFM. Overall, the influence of t_{plasma} on the surface roughness and crystallinity is similar to the previously reported impact of increasing substrate temperature, which favors formation of nanocrystalline Co_3O_4 films[16], and the general trend of more crystalline films with PE-ALD processes.[24]

The electrochemical performance characteristics and stability of PE-ALD grown CoO_x thin films as a function of t_{Plasma} and P_{plasma} were determined by linear sweep voltammetry (LSV) and chronopotentiometry (CP) in 1 M NaOH (pH 13.3) without illumination (Fig. 2b and S3). The lowest plasma exposure time of 5 s exhibits a negligible current density and is highly unstable under OER conditions. For longer exposure times, the OER activity increases up to t_{plasma} = 15 s and then decreases for longer exposure times. The t_{plasma} dependence is also reflected by the corresponding overpotential necessary to achieve a current density of 1 mA cm^{-2} (inset Fig. 2b). For a pulse time of 15 s, an overpotential of 361 mV is achieved, while a current density of 39.9 mA cm^{-2} is measured at 1.8 V versus reversible hydrogen electrode (RHE), in good agreement with a previous study of PE-ALD grown CoO_x films.[15] For t_{plasma} = 10 s, complementary CP measurements show an increase in the potential after less than 20 s, which indicates material degradation during operation (inset Fig. 2c). For t_{Plasma} of 15 s, 20 s, and 90 s, the potential remains constant for 1 h (Fig. 2c), indicating good electrochemical stability. A similar effect is also observed for increasing plasma powers at a fixed plasma exposure time of 5 s (Fig. S3), where the best stability and highest OER performance is obtained for 50 W. Accordingly, short t_{plasma} and low P_{plasma} are beneficial for improved OER activity of the films, while longer t_{plasma} and high P_{plasma} enhance the material stability under operating conditions. This finding highlights the importance of controlling deposition parameters to achieve a favorable balance between activity and stability. As described below, an improved understanding of the underlying mechanisms of PE-ALD growth-induced CoO_x phase formation indeed enables a targeted synthesis of highly active and stable CoO_x catalyst layers.

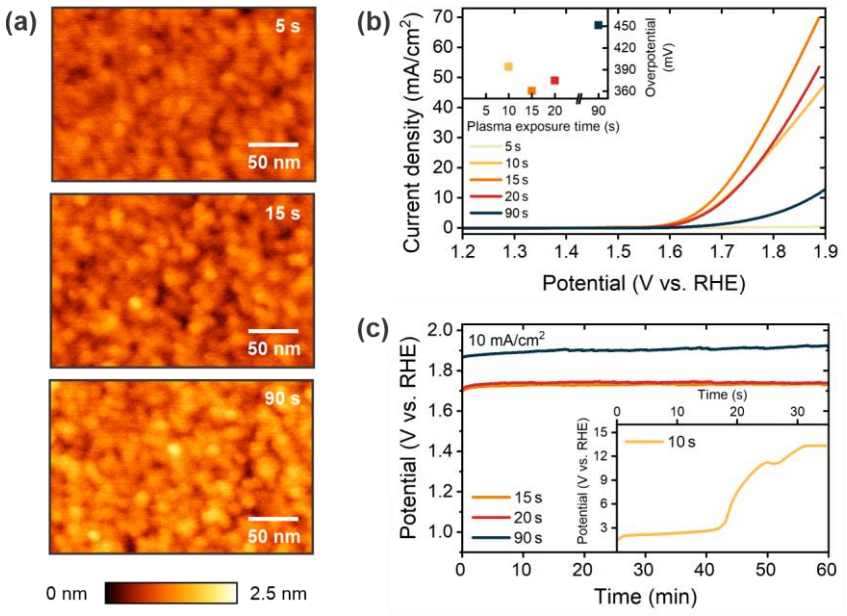

Figure 2. Morphology, electrochemical performance and stability of CoO_x films grown on p^+-Si with increasing plasma exposure times. (a) Atomic force microscopy images of PE-ALD grown CoO_x films for t_{plasma} = 5 s, 15 s, and 90 s. (b) Linear sweep voltammetry and (inset) overpotential necessary to achieve a current density of 1 mA cm^{-2} for samples deposited using a fixed 10 W oxygen plasma power with increasing exposure times ranging from 5 s to 90 s. (c) Chronopotentiometry measurements recorded at 10 mA cm^{-2} for 1 h for t_{plasma} between 15 s and 90 s. The inset in (c) shows the chronopotentiometry measurements for a sample grown with a shorter pulse time of 10 s, which experiences rapid degradation. For a pulse time of 5 s, the electrode degraded immediately (not shown).

Chemical Composition and Phase Control

Both t_{plasma} and P_{plasma} have a similar impact on the PE-ALD growth process, as well as on the electrochemical activity and the chemical stability of the deposited CoO_x films. To decouple these influences, we varied t_{plasma} at constant P_{plasma} and thereby investigated the dependency of the chemical composition on plasma exposure times. We analyzed the surface and bulk compositions for different t_{plasma} by X-ray photoelectron spectroscopy (XPS) and X-ray absorption near-edge structure spectroscopy (XANES), respectively. Figure 3 shows the XPS core-level spectra of Co $2p_{3/2}$, O 1s, and C 1s for t_{plasma} = 5 s, 15 s, and 90 s, reflecting the main compositional changes on the surface. The Co $2p_{3/2}$ spectra (Fig. 3a) can be deconvoluted into two main oxide components, namely Co_3O_4 (mixed valent Co^{2+}/Co^{3+}, orange) and $Co(OH)_2$ (Co^{2+}, blue), using the multiplet splitting approach by Biesinger et al.[25]. For oxidation pulses of 5 s, the chemical composition is dominated by $Co(OH)_2$. For longer exposure times, the contribution of $Co(OH)_2$ decreases (Fig. 3d) and the formation of a Co_3O_4 layer is observed. For t_{plasma} = 90 s, the thin film is mainly composed of Co_3O_4 with a minor contribution from $Co(OH)_2$. These findings are further supported by valence band (VB) spectroscopy (Fig. S4). For t_{plasma} = 5 s, the VB exhibits features at 2.1 eV and 3.8 eV arising from octahedral Co^{2+} from $Co(OH)_2$ and from tetrahedral Co^{2+} from the spinel Co_3O_4 phase. For increasing t_{plasma}, the VB is dominated by features at 1.2 eV and 3.8 eV corresponding to octahedral Co^{3+} and tetrahedral Co^{2+}, respectively, from the mixed valent spinel Co_3O_4 phase.[19] Accordingly, extending the plasma exposure time facilitates the formation of a Co_3O_4 interface layer.

The O 1s spectra (Fig. 3b) are composed of lattice oxygen (orange), hydroxides (blue), and adsorbed water (yellow). For increasing t_{plasma}, the contribution of lattice oxygen increases while the hydroxide component decreases. These chemical changes are consistent with the significantly higher $Co(OH)_2$ contribution for shorter plasma exposure times, as observed in the Co $2p_{3/2}$ spectra (Fig. 3a).

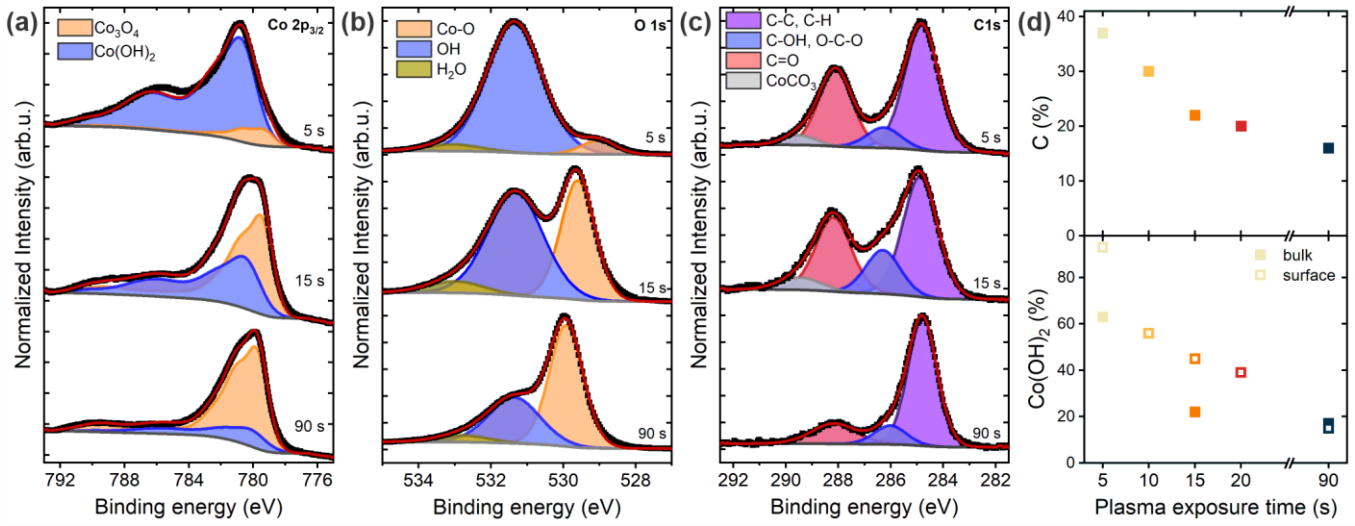

Figure 3. Chemical composition of PE-ALD-grown CoO_x films. High-resolution XPS core level spectra of Co $2p_{3/2}$ (a), O 1s (b), and C 1s (c) as a function of t_{plasma} with a fixed plasma power of 10 W. (d) Atomic contribution of carbon impurities and $Co(OH)_2$ to the film composition. The $Co(OH)_2$ percentage at the surface was extracted from the XPS Co $2p_{3/2}$ spectra, whereas the bulk contribution was established by fitting a linear combination of references spectra to the XANES data.

The $CoCp_2$ precursor is a metalorganic compound, which consists of two cyclopentadienyl anions ($C_5H_5^-$) bound to a Co center. Thus, carbon residuals from the precursor molecule are likely to be incorporated during the PE-ALD growth process. Therefore, we additionally analyzed the C 1s spectrum (Fig. 3c) to quantify the carbon impurities as a function of t_{plasma} for a fixed plasma power of 10 W. In addition to peaks associated with C-C (284.8 eV, purple), C–OH (~286.2 eV, blue), and C=O (~288.2 eV, red), a comparatively weak peak at 289.4 eV (grey) is present for $t_{Plasma} \leq 15$ s, which could indicate the formation of $CoCO_3$.[26] Previous studies revealed the formation of gaseous carbon oxide species during the plasma exposure time and thus, a combustion-like reaction of oxygen radicals with the precursor.[16,20] In the present case, we find that short oxidation times lead to an incomplete reaction and the formation of a minority content of $CoCO_3$ within the films. The peak at 289.4 eV is not present in the C 1s spectrum for t_{Plasma} = 90 s, which agrees with the prolonged oxidation of the precursor. The highest content of carbon impurities

within the film is determined for shortest exposure times of 5 s, and decreases for longer values of t_{plasma} (Fig. 3d and Table S1). Accordingly, short values of t_{plasma} lead to an incomplete decomposition of the $C_5H_5^-$ ligands resulting in higher carbon impurity concentrations within the PE-ALD films. For the two shortest plasma oxidation times, the carbon content is especially high (≥ 30 at. %), which correlates with the observed poor chemical stability (Fig. 2) and an increased disorder (Fig. S2). Furthermore, this observation agrees with the VB spectra (Fig. S4) and is additionally supported by extended X-ray absorption fine structure (EXAFS) spectra (Fig. S5), which reveal the absence of any long-range order in the sample grown with 5 s plasma exposure time. Thus, the effect of short oxygen plasma exposure times is similar to the effect of reduced substrate temperatures during PE-ALD grown CoO_x films[15,16,18], which have been shown to have higher carbon content. In contrast, for plasma exposure times of 15 s or longer, the carbon content is significantly lower and gradually decreases with increasing t_{plasma}.

Complementary XANES measurements were performed (Fig. S6) to determine the bulk composition of the films (Fig. 3d). A linear combination of the Co_3O_4 and $Co(OH)_2$ reference spectra were used to fit the data. This analysis reveals a decreasing $Co(OH)_2$ content from 63% to 17% for increasing plasma exposure times (Table S1). Compared to the surface-dominated XPS measurements, the XANES data reveal lower $Co(OH)_2$ contributions in the bulk of the thin film. This comparison supports our conclusion that $Co(OH)_2$ preferentially forms on the film surface. Overall, the improved electrochemical stability for longer plasma exposure times agrees with the formation of a Co_3O_4 interface layer possessing a reduced carbon content, while the improved electrochemical activity correlates with the contribution of the $Co(OH)_2$ surface layer. These findings are in agreement with a recent operando study reported that $Co(OH)_2$ promotes the formation of CoOOH under OER conditions, thereby improving the catalytic activity of electrodes possessing $Co(OH)_2$ surface layers.[19]

Physical, Mechanical and Optical Properties

To further understand the impact of t_{Plasma} on the physical film properties, XRR measurements were carried out to determine the density and thickness of the CoO_x films (Fig. 4). Except for the sample with t_{plasma} = 90 s, the XRR data were simulated with a bilayer model with a $Co(OH)_2$ surface and a Co_3O_4 interface layer according to the XPS and XANES results. For longer t_{plasma}, the density and thickness of the $Co(OH)_2$ layer decrease, while they increase for the Co_3O_4 interface layer (Fig. 4a-b). For t_{plasma} = 90 s the density is 6.5 g cm^{-3}, which agrees with the reported Co_3O_4 bulk value of 6.1 g cm^{-3} as well as with previously reported densities for ALD-grown Co_3O_4 films[16]. A similar densification has previously been reported for different PE-ALD-grown metal oxides for increasing deposition temperatures and plasma exposure times.[27] For $t_{plasma} \geq 15$ s, the XRR results show that the PE-ALD grown CoO_x layers are composed of a thicker (≥ 6 nm), dense Co_3O_4 interface and a rather thin (≤ 1 nm), highly porous $Co(OH)_2$ surface layer.

To elucidate the nanomechanical and adhesion properties, we performed local scratching experiments using AFM. The applied force was adjusted to selectively remove the CoO_x (Fig. 4c) film without impacting the underlying Si substrate (Fig. S7). We observe that the force that is necessary to remove the CoO_x films increases for increasing plasma exposure times. Specifically, 0.6 µN and 4.5 µN are required to remove the films for t_{plasma} = 5 s and 15 s, respectively. For t_{plasma} = 90 s, the required force is significantly higher, causing the simultaneous removal of both CoO_x and Si. The nanoscratching tests indicate that the films grown with shorter t_{plasma} are structurally more fragile and exhibit reduced adhesion to the supporting structure compared to films deposited with longer t_{plasma}. The reduced hardness of the CoO_x films (Fig. S8) for short plasma exposure times agrees with reduced density, increased disorder, and increased carbon incorporation as observed by XRR, XRD, and XPS, respectively. Furthermore, the low adhesion to the supporting structure likely contributes to the chemical instability of CoO_x under OER conditions.

For their application as protection layers in PEC energy conversion devices, the optical properties of catalyst layers can have a significant effect on the overall performance and efficiency, since they are often non-transparent, and can block light from reaching the underlying semiconductor light absorber due to parasitic light absorption. Therefore, we conducted *ex-situ* variable angle spectroscopic ellipsometry on the PE-ALD grown CoO_x films to determine the refractive index, *n*, and extinction coefficient, *k*, as a function of the plasma exposure time (Fig. 4d-e). The optical constants were extracted by fitting the VASE data with a general oscillator model as described in Ref [16] for Co_3O_4. Here, we note that it was necessary to apply a single layer model, since the measured ellipsometry parameters Ψ and Δ do not provide sufficient information to unambiguously fit the optical constants for two layers, especially given

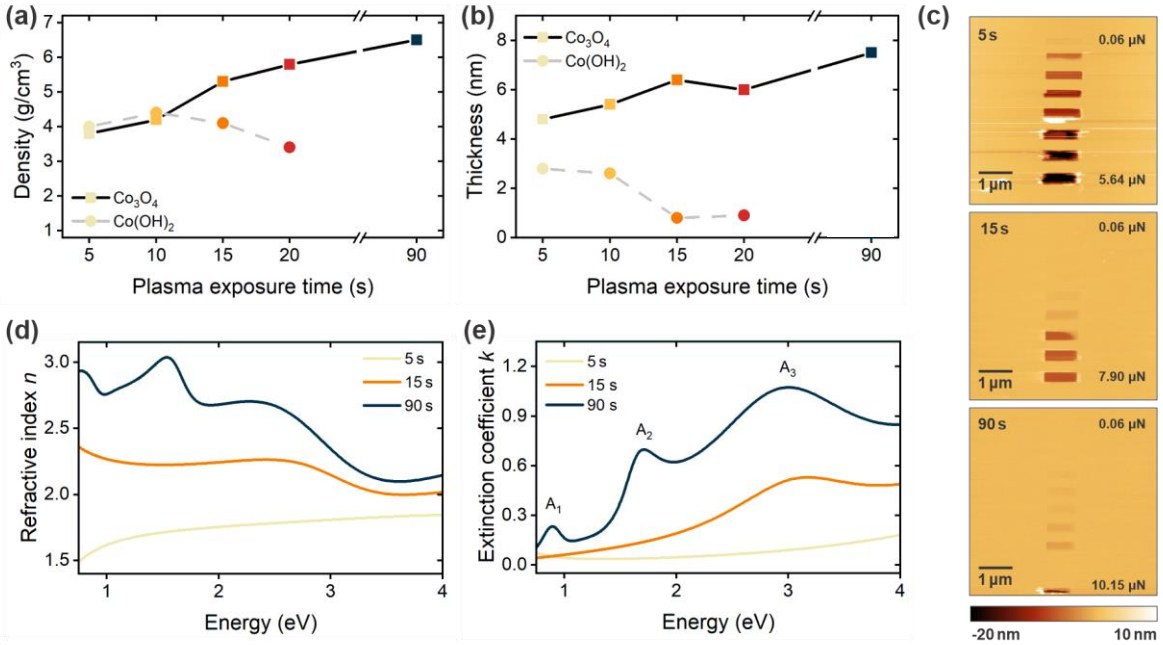

Figure 4. Density, thickness, and growth characteristics of PE-ALD grown CoO_x thin films using different plasma exposure times. Density (a) and film thickness (b) for different t_{plasma} determined by X-ray reflectivity measurements and modeled with $Co(OH)_2$ surface and Co_3O_4 interface layers. (c) AFM images of nanomechanical scratching experiments on CoO_x films grown with t_{plasma} = 5 s, 15 s, and 90 s, whereby the applied force is continuously increased from 0.06 µN to 5.64 µN, 7.90 µN, and 10.15 µN, respectively. Optical properties *n* (d) and *k* (e) of the CoO_x films as function of t_{plasma}.

the low total content of $Co(OH)_2$ for longer plasma exposure times. Therefore, we refer to *n* and *k* only as pseudo-optical constants. For increasing plasma exposure times, the dielectric constants increase in magnitude, indicating higher densities and a convergence to the ideal optical properties of Co_3O_4. [16,28] The increased visible light absorption with plasma exposure time, determined by fitting ellipsometry data (Fig. 4d), is consistent with transmittance measurements on fused silica (Fig. S9). For t_{plasma} = 90 s, the values for *n* and *k* of the PE-ALD-grown Co_3O_4 films are in good agreement with previous studies on Co_3O_4 films.[16,23,28] In detail, the obtained Co_3O_4 film is characterized by absorption bands at 0.9 eV (A_1), 1.6 eV (A_2), and 2.9 eV (A_3) (Fig. 4e). These features match the reported complex dielectric function of Co_3O_4 and have been assigned to charge transfer between $Co^{2+} \rightarrow Co^{3+}$ (A_1), the reverse charge transfer $Co^{3+} \rightarrow Co^{+2}$ (A_2), and the ligand to metal charge transfer between $O^{2-} \rightarrow Co^{2+}$ (A_3).[16,29] For shorter exposure times, the optical transitions A_1 and A_2 at lower energies vanish. These absorption features involve Co^{3+} cations, which are only present in the spinel structure of Co_3O_4. Accordingly, the change in optical properties reflects the change in chemical composition from Co_3O_4 dominated films for prolonged t_{plasma} to films with a high $Co(OH)_2$ contribution for short t_{plasma}, as observed by XPS and XANES. For intermediate plasma exposure times, these results highlight the potential application of CoO_x layers as catalytic protection layers for semiconductor light absorbers in PEC devices, since they are highly stable in harsh chemical environments, catalytically active, and have only a minimal effect on the transmitted light intensity, which reduces parasitic light absorption.

Design of bilayer films for improved electrochemical performance

Having established the relation between the PE-ALD growth process and structural, chemical, and functional properties of the grown CoO_x films, we intentionally designed bilayer films with improved electrochemical properties. In a two-step growth process, we first used long plasma exposure times of 20 s to grow a compact Co_3O_4 interface layer, which provides good adhesion to the underlying substrate and chemically stability under operation conditions, while forming a continuous transition to the upper catalytic layer. Second, we applied short plasma exposure times of 10 s to deposit an amorphous $Co(OH)_2$ surface layer, which improves the catalytic activity for OER. We used in total 100 PE-ALD cycles for the film deposition, similar to the growth of biphasic layers above, and optimized the ratio between both layers for the highest electrochemical performance (Fig. 5). Bilayers deposited with 30 cycles of t_{plasma} = 20 s and 70 cycles of t_{plasma} = 10 s improved performance at high current densities relevant for electrochemical energy conversion (Fig. 5a) and similar electrochemical stability at moderate current densities

(Fig. 5b). Compared to t_{plasma} = 90 s, the application of t_{plasma} = 20 s for the growth of the interface layer has the advantage to reduce substrate oxidation and form good adhesion to the $Co(OH)_2$ surface layer. These findings indicate that only an ultra-thin interface layer is required to chemically protect the underlying substrate, while at the same time permitting efficient interfacial charge transport.

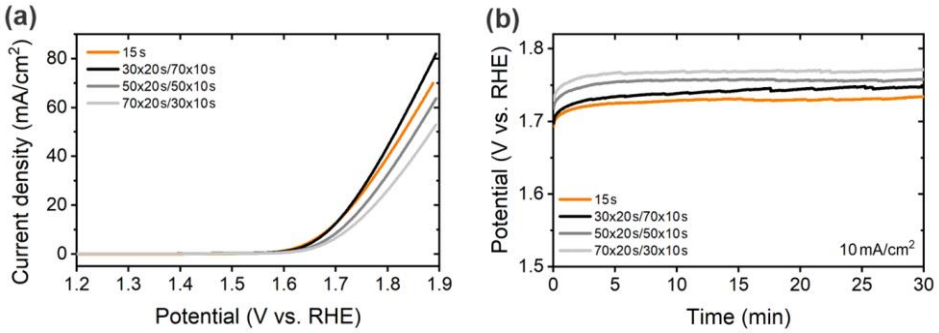

Figure 5. Electrochemical performance and stability of CoO_x bilayers grown on p^+-Si for different plasma exposure time ratios. (a) Linear sweep voltammetry for samples deposited using a fixed 10 W oxygen plasma power and different ratios of t_{plasma} = 20 s and 10 s. (b) Corresponding chronopotentiometry measurements recorded at 10 mA cm^{-2} for 30 min comparing the best biphasic film with t_{plasma} = 15 s and the intentionally grown bilayers.

Conclusion

In summary, we have shown that the plasma exposure time and plasma power can be used in low-temperature PE-ALD processes to tune the composition, structure, mechanical, and optical properties of CoO_x electrodes, thereby enabling control over their electrochemical stability and activity. For short plasma exposure times, the deposited films are composed of mainly $Co(OH)_2$ and are catalytically active for OER, but their properties are impacted by the incorporation of high concentrations of carbon impurities. Specifically, the films exhibit low hardness and poor adhesion to the underlying substrate, which causes poor stability under OER conditions. In contrast, long plasma exposure times of 90 s facilitate the complete oxidation of the adsorbed cobaltocene precursor to Co_3O_4 and reduce the carbon impurity concentrations within the films. While these conditions yield Co_3O_4 films that are dense, have improved crystallinity, and show enhanced adhesion to the underlying substrate, they also result in increased oxidation of chemically sensitive substrates. This combination of properties renders these films highly stable under OER conditions, but lead to low OER activities. The best compromise between stability and activity is observed for intermediate plasma exposure times and plasma powers, leading to the formation of a biphasic layer consisting of a catalytically active $Co(OH)_2$ surface and a chemically stable Co_3O_4 interface layer. These films have the additional advantage of a relatively low light absorption, which makes them suitable as protective catalytic layers on semiconductors for the application in PEC devices. Finally, we leveraged the established relation between deposition parameters and functional properties of CoO_x films to develop a two-step PE-ALD process for the design of bilayer films with improved electrochemical performance without compromising stability. The mechanistic insights into the PE-ALD processes gained through this work enable controlled phase engineering of multi-functional catalysts at low substrate temperatures. We envision that the developed understanding of biphasic thin films can be extended to other (metallocene-based) ALD processes for the design of novel functional coatings relevant for various applications, including electrocatalytic energy conversion, supercapacitor-based electrochemical energy storage, and even memristor technologies based on solid state redox reactions.

Experimental section

Thin film synthesis. Multifunctional cobalt oxide thin films were deposited by PE-ALD (Fiji G2, Veeco Instruments Inc.) on degenerately doped p^+-type (< 0.005 Ohm cm, <100>, Siegert Wafer GmbH) Si substrates with native oxide, as well as on fused silica wafers (Siegert Wafer GmbH). Prior to deposition, the substrates were cleaned consecutively in acetone and isopropanol for 5 min each using an ultrasonic bath. Before each deposition, the wall of the PE-ALD system was coated with 50 cycles of Al_2O_3 (TMA/H_2O) to avoid cross-contamination from previous processes.
For the CoO_x deposition, $CoCp_2$ (98% Strem Chemicals) was used as the cobalt precursor and oxygen plasma (purity 6.0 oxygen gas, Linde) as the oxidant. The precursor lines, carrier gas lines, and the reactor walls were heated to 100 °C. The $CoCp_2$ bubbler was heated to 80 °C and bubbled with an Ar flow (purity 6.0, Linde) of 60 sccm. The cobaltocene precursor was deposited on the substrate surface during the first half cycle, consisting of 5 s $CoCp_2$ dosing and 5 s purging. In the second half-cycle, the precursor was oxidized by exposing it to a highly reactive oxygen plasma using an oxygen gas flow of 20 sccm. During this process step, a 5 s settling time was required to establish stable flow and plasma power conditions. To tune catalytic activity, chemical stability, and physical properties of the CoO_x films, the plasma exposure time (t_{plasma}) was increased from a minimum of 5 s up to 90 s using a fixed plasma power of 10 W, and the purge time was set to 10 s. In a separate series, the plasma power was varied from 10 W to 300 W using a constant t_{plasma} of 5 s and an identical purge time of 10 s. For each film, the chamber pressure during deposition was maintained at 0.1 mbar with a constant Ar background flow of 110 sccm. For all reactor conditions, 100 cycles were used to deposit the films.

Structural and morphological characterization. X-ray photoelectron spectroscopy (XPS) was conducted to analyze the near-surface composition using a monochromatic Al K_α source ($h\nu$ = 1486.6 eV) and a hemispherical analyzer with a pass energy of 20 eV (Phoibos 150, SPECS). XPS binding energies were corrected by shifting the C 1s core level position to 284.8 eV. Spectral fitting was conducted using the Casa XPS analysis software. The Co $2p_{3/2}$ spectra were fitted using parameters from Ref.[25].
The film morphology was determined by atomic force microscopy using a Bruker Dimension Icon under ambient conditions. Measurements were performed in PeakForce mode using a cantilever with a spring constant of 3.0 N m^{-1} (RFESPA, Bruker). Data post-processing was performed with Gwyddion. Nano scratching experiments were performed with a Multimode V microscope (Bruker) in ambient using diamond-like carbon probes (Tap190DLC, BudgetSensors) with a nominal radius of 15 nm in contact mode. The tip-sample force, F_{ts}, in hard contact with the surface, was calculated using Hooke's law, $F_{ts} = ks$, where the measured deflection, s, was determined from a force-distance curve and the spring constant, k, was obtained from a thermal tune. Nano scratching was performed in ~1 μm×0.5 μm^2 windows with 512 sampling points and a scan rate of 0.3 Hz. Tapping mode height images (5×5 μm^2 and 3×3 μm^2) were acquired from the same sample region before and after every scratching experiment at a scan rate of 0.5 Hz with 512-point sampling.
X-ray reflectivity (XRR) measurements were conducted using an X-ray diffractometer (SmartLab, Rigaku) with Cu K_α radiation. The $2\theta/\omega$ angle was scanned between 0 – 4° with 0.01° step size. Grazing incidence X-ray diffraction was performed with the same instrument using 1° grazing incident angle, while the 2θ diffraction angle was scanned between 15 – 70° with 0.02° step size.

Optical characterization. Variable angle spectroscopic ellipsometry was conducted using a J.A. Woollam M-2000X ellipsometer. Ψ and Δ were measured over a spectral range from 310 nm to 1690 nm at reflection angles of 55°, 65°, and 75° for *ex-situ* and 65° for *in-situ* measurements during the ALD process. Analysis of the data was performed with the CompleteEASE software. The optical constants were extracted by fitting the VASE data with a general oscillator model as described in Ref.[16] and[28] for Co_3O_4.
The Co K-edge X-ray absorption near-edge structure (XANES, 7600-7800 eV) and extended X-ray absorption fine structure (EXAFS, 7800-8450 eV) measurements were carried out at the KMC-2 beamline at the BESSY II operated by the Helmholtz-Zentrum Berlin für Materialien und Energie. For all measurements a graded Si−Ge(111) double-crystal monochromator was used. The intensity of the primary beam was stabilized using a SIS2900 D-MOSTAB (SISGmbH) monochromator stabilizer. All experiments were conducted at ambient conditions. Along with the cobalt oxide samples, a Co foil was simultaneously measured as reference. As oxide reference samples, multiple layers of bulk $Co(OH)_2$ and Co_3O_4 (Sigma Aldrich) powder affixed to adhesive Kapton tape were used. All standards were

measured in transmission mode using ionization chambers placed before and after the standards to provide incident and transmitted intensities, I_0 and I_T, respectively. The Athena software was used to remove pre-edge and post-edge contributions and to normalize the data to the edge step. Each spectrum was energy calibrated by using the second derivative of the corresponding Co reference absorption spectrum. The bulk composition was calculated from the XANES region by linear combination fitting the $Co(OH)_2$ and Co_3O_4 reference spectra to the sample spectra. The Fourier transformation into real space was computed using a Hanning window from 3 to 11.9 $Å^{-1}$ in k-space.

Electrochemical measurements. Electrochemical measurements were performed in a three-electrode setup using an Ag/AgCl reference electrode (3 M KCl, Dri-Ref-2SH, WPI Europe), the cobalt oxide films as working electrodes, and a Pt wire as counter electrode. Cyclic voltammetry and chronopotentiometry were conducted in 1 M NaOH at pH 13.3 under dark conditions using a Gamry potentiostat (Reference 600). The working electrodes were fabricated by scratching the backside of the p^+-Si and adding conductive indium-gallium eutectic (Sigma-Aldrich). A Cu wire was attached to the backside using silver epoxy (Circuit Works). The wire was covered with a glass tube and subsequently sealed using a silicone polymer compound (101RF BLACK, Microset).

Acknowledgements

We acknowledge support from the Deutsche Forschungsgemeinschaft (DFG, German Research Foundation) under Germany´s Excellence Strategy – EXC 2089/1 – 390776260. J.E. acknowledges funding by the Deutsche Forschungsgemeinschaft (DFG, German Research Foundation) – 428591260 and support from the Bavarian Academy of Sciences and Humanities. L.I.W. and V.S. were supported by the European Research Council (ERC) under the European Union's Horizon 2020 research and innovation programme (grant agreement No. 864234). L.H. received support from TUM.Solar in the context of the Bavarian Collaborative Research Project Solar Technologies Go Hybrid (SolTech). We thank the Helmholtz-Zentrum Berlin für Materialien und Energie for the allocation of synchrotron radiation beamtime.

References

1. Montoya, J. H. *et al.* Materials for solar fuels and chemicals. *Nat. Mater.* **16**, 70–81 (2017).
2. Hydrogen on the rise. *Nat. Energy* **1**, 1–1 (2016).
3. Lewis, N. S. & Nocera, D. G. Powering the planet: Chemical challenges in solar energy utilization. *Proc. Natl. Acad. Sci.* **103**, 15729–15735 (2006).
4. Roger, I., Shipman, M. A. & Symes, M. D. Earth-abundant catalysts for electrochemical and photoelectrochemical water splitting. *Nat. Rev. Chem.* **1**, 1–13 (2017).
5. Burke, M. S., Enman, L. J., Batchellor, A. S., Zou, S. & Boettcher, S. W. Oxygen Evolution Reaction Electrocatalysis on Transition Metal Oxides and (Oxy)hydroxides: Activity Trends and Design Principles. *Chem. Mater.* **27**, 7549–7558 (2015).
6. Jiao, Y., Zheng, Y., Jaroniec, M. & Zhang Qiao, S. Design of electrocatalysts for oxygen- and hydrogen-involving energy conversion reactions. *Chem. Soc. Rev.* **44**, 2060–2086 (2015).
7. Indra, A. *et al.* Unification of Catalytic Water Oxidation and Oxygen Reduction Reactions: Amorphous Beat Crystalline Cobalt Iron Oxides. *J. Am. Chem. Soc.* **136**, 17530–17536 (2014).
8. Koza, J. A., He, Z., Miller, A. S. & Switzer, J. A. Electrodeposition of Crystalline Co_3O_4 — A Catalyst for the Oxygen Evolution Reaction. *Chem. Mater.* **24**, 3567–3573 (2012).
9. Toma, F. M. *et al.* Mechanistic insights into chemical and photochemical transformations of bismuth vanadate photoanodes. *Nat. Commun.* **7**, 12012 (2016).
10. Eichhorn, J. *et al.* Revealing Nanoscale Chemical Heterogeneities in Polycrystalline Mo-$BiVO_4$ Thin Films. *Small* **16**, 2001600 (2020).
11. W. Ager, J., R. Shaner, M., A. Walczak, K., D. Sharp, I. & Ardo, S. Experimental demonstrations of spontaneous, solar-driven photoelectrochemical water splitting. *Energy Environ. Sci.* **8**, 2811–2824 (2015).
12. Montoya, J. H. *et al.* Materials for solar fuels and chemicals. *Nat. Mater.* **16**, 70–81 (2017).
13. Hufnagel, A. G. *et al.* Electron-Blocking and Oxygen Evolution Catalyst Layers by Plasma-Enhanced Atomic Layer Deposition of Nickel Oxide. *Adv. Mater. Interfaces* **5**, 1701531 (2018).
14. Omerzu, A. *et al.* Large enhancement of photocatalytic activity in ZnO thin films grown by plasma-enhanced atomic layer deposition. *Surf. Interfaces* **23**, 100984 (2021).
15. Yang, J. *et al.* A multifunctional biphasic water splitting catalyst tailored for integration with high-performance semiconductor photoanodes. *Nat. Mater.* **16**, 335–341 (2017).

16. Donders, M. E., Knoops, H. C. M., Sanden, van de, M. C. M., Kessels, W. M. M. & Notten, P. H. L. Remote plasma atomic layer deposition of Co_3O_4 thin films. *J. Electrochem. Soc.* **158**, G92–G96 (2011).
17. Singh, A. K., Adstedt, K., Brown, B., Singh, P. M. & Graham, S. Development of ALD Coatings for Harsh Environment Applications. *ACS Appl. Mater. Interfaces* **11**, 7498–7509 (2019).
18. Yang, J. *et al.* Efficient and Sustained Photoelectrochemical Water Oxidation by Cobalt Oxide/Silicon Photoanodes with Nanotextured Interfaces. *J. Am. Chem. Soc.* **136**, 6191 (2014).
19. Favaro, M. *et al.* Understanding the Oxygen Evolution Reaction Mechanism on CoO_x using Operando Ambient-Pressure X-ray Photoelectron Spectroscopy. *J. Am. Chem. Soc.* **139**, 8960–8970 (2017).
20. Di Palma, V., Knoops, H. C. M., Kessels, W. M. M. (Erwin) & Creatore, M. Atomic layer deposition of cobalt phosphate from cobaltocene, trimethylphosphate, and O_2 plasma. *J. Vac. Sci. Technol. A* **38**, 022416 (2020).
21. Ha, S.-C., Choi, E., Kim, S.-H. & Sung Roh, J. Influence of oxidant source on the property of atomic layer deposited Al_2O_3 on hydrogen-terminated Si substrate. *Thin Solid Films* **476**, 252–257 (2005).
22. Knoops, H. C. M., de Peuter, K. & Kessels, W. M. M. Redeposition in plasma-assisted atomic layer deposition: Silicon nitride film quality ruled by the gas residence time. *Appl. Phys. Lett.* **107**, 014102 (2015).
23. Holden, K. E. K. & Conley, J. F. Characterization of atomic layer deposited semiconducting Co_3O_4. *J. Vac. Sci. Technol. A* **37**, 020903 (2019).
24. Miikkulainen, V., Leskelä, M., Ritala, M. & Puurunen, R. L. Crystallinity of inorganic films grown by atomic layer deposition: Overview and general trends. *J. Appl. Phys.* **113**, 021301 (2013).
25. Biesinger, M. C. *et al.* Resolving surface chemical states in XPS analysis of first row transition metals, oxides and hydroxides: Cr, Mn, Fe, Co and Ni. *Appl. Surf. Sci.* **257**, 2717–2730 (2011).
26. Blanchard, D. L. & Baer, D. R. The interactions of Co, Mn and water with calcite surfaces. *Surf. Sci.* **276**, 27–39 (1992).
27. Lapteva, M. *et al.* Influence of temperature and plasma parameters on the properties of PEALD HfO_2. *Opt. Mater. Express* **11**, 1918–1942 (2021).
28. Qiao, L. *et al.* Nature of the band gap and origin of the electro-/photo-activity of Co_3O_4. *J. Mater. Chem. C* **1**, 4628–4633 (2013).
29. Athey, P. R., Urban, F. K., Tabet, M. F. & McGahan, W. A. Optical properties of cobalt oxide films deposited by spray pyrolysis. *J. Vac. Sci. Technol. A* **14**, 685–692 (1996).